Title: Compelling Evidence for a Large Exomoon Orbiting Kepler-1625b

Authors: Alex Teachey,[1*] David M. Kipping[1]

Affiliations: [1]Department of Astronomy, Columbia University in the City of New York

[*]E-mail: ateachey@astro.columbia.edu.

One Sentence Summary: HST finds evidence for a large exomoon.

Abstract: Exomoons are the natural satellites of planets orbiting stars outside our Solar System. We present new observations of a candidate exomoon in the Kepler-1625b system using the Hubble Space Telescope, carried out on 28-29 October 2017 to validate or refute the moon's presence. We find compelling evidence in favor of the moon hypothesis, based on timing deviations and a reduced flux from the star consistent with a large transiting exomoon. Self-consistent photodynamical modeling suggests that the planet is likely several times the mass of Jupiter, while the exomoon has a mass and radius akin to that of Neptune. If confirmed this represents the first unambiguous detection of a moon beyond our Solar System.

Main Text: The search for exomoons remains in its infancy. To date, there are no confirmed exomoons in the literature, although an array of techniques have been proposed to detect their existence, such as microlensing (*1–3*), direct imaging (*4,5*), cyclotron radio emission (*6*), pulsar timing (*7*) and transits (*8–10*). The transit method is particularly attractive however since many small planets down to lunar radius have already been detected (*11*), and transits afford repeated observing opportunities to further study candidate signals.

Previous searches for transiting moons have established that Galilean-sized moons are uncommon at semi-major axes of 0.1 to 1 AU (*12*). This result is consistent with theoretical work which has shown that the shrinking Hill sphere (*13*) and potential capture into evection resonances (*14*) during a planet's inward migration could efficiently remove primordial moons. Nevertheless, amongst a sample of 284 transiting planets recently surveyed for moons, one planet did show some evidence for a large satellite, Kepler-1625b (*12*). The planet is a Jupiter-sized validated world (*15*) orbiting a Solar-mass star (*16*) close to 1 AU in a likely circular path (*12*), making it a prime *a priori* candidate for moons. Based on this, and the hints seen in the three transits observed by *Kepler*, we requested and were awarded time on the Hubble Space Telescope (HST) to observe a fourth transit expected on 28-29 October 2017. In this work, we report on these new observations and their impact on the exomoon hypothesis for Kepler-1625b.

Our original analysis was the product of a multi-year survey and thus utilized an earlier version of the processed photometry released by the *Kepler* Science Operations Center (SOC). In that study (*12*), we used the Simple Aperture Photometry (`SAP`) from SOC pipeline version 9.0 (*17*), but the most recent and final data release uses version 9.3. In this work we have re-analyzed the *Kepler* data using the revised photometry, which includes updated aperture contamination factors that also affect our analysis. During this process, we also investigated the effect of varying the model used to remove long-term trend present in the *Kepler* data.

We detrended the revised *Kepler* photometry using five independent methods. The first

method is the CoFiAM algorithm (*18*) which was the approach used in the original study, since it was specifically designed with exomoon detection in mind. In addition, we considered four other popular approaches: a polynomial fit, a local line fit, a median filter, and a Gaussian process (see the Supplementary Materials for a detailed description of each). The detrended photometry is stable across the different methods (see Figure 1), with a maximum standard deviation between any two SAP time series of 250 ppm, far below the median formal uncertainty of ~ 590 ppm. Although we verified the Presearch Data Conditioning (PDC) version of the photometry (*19, 20*) produces similar results (as evident in Figure 1), we ultimately only use the five SAP reductions in what follows. We produce a "method marginalized" final time series by taking the median of the $i^{\rm th}$ datum across the five methods and propagating the variance between them into a revised uncertainty estimate (see the Supplementary Materials for details). In this way, we produce a robust correction of the *Kepler* data accounting for differences in model assumptions.

We fit photodynamical models (*21*) to the revised *Kepler* data, using the updated contamination factors from SOC v9.3, prior to introducing the new HST data. Bayesian model selection reveals only a modest preference for the moon model, with the Bayes factor (K), going from $2 \log K = 20.4$ in our original study down to just 1.0 now. Detailed investigation reveals that this is not due to our new detrending approach, as we applied our method marginalized detrending to the original v9.0 data and recovered a similar result to our original analysis (see the Supplementary Materials for details). Instead, it appears that the reduced evidence is largely caused by the changes in the SAP photometry going from v9.0 to v9.3, and to a lesser degree by the new contamination factors. This can be seen in Figure 1, where the third transit in particular experiences a pronounced change between the two versions, and it was this epoch which displayed the greatest evidence for a moon-like signature in the original analysis.

With a much larger aperture than *Kepler*, HST is expected to provide several times more pre-

cise photometry. Accordingly, the question as to whether Kepler-1625b hosts a large moon or not should incorporate this new information and in what follows we describe how we processed the HST data and then combined it with the revised *Kepler* photometry.

HST monitored the transit of Kepler-1625b occurring on 28-29 October, 2017 with Wide Field Camera 3 (WFC3). A total of 26 orbits, amounting to some 40 hours, were devoted to observing the event. The observations consisted of one direct image and 232 exposures using the G141 grism, a slitless spectroscopy instrument that projects the star's spectrum across the CCD. This provides spectral information on the target in the near-infrared from approximately 1.1 to 1.7 microns. Of these 232 exposures, only three were unusable, as they coincided with the spacecraft's passage through the South Atlantic Anomaly, at which time HST is forced to use its less-accurate gyroscopic guidance system. Each exposure lasted roughly 5 minutes, resulting in about 45 minutes on target per orbit. Images are extracted using standard tools made available by the Science Telescope Space Institute (STScI) and are described in the Supplementary Materials.

Native HST time stamps, recorded in the Modified Julian Date ($\mathrm{MJD_{UTC}}$) system, were converted to Barycentric Julian Date ($\mathrm{BJD_{UTC}}$) for consistency with the *Kepler* time stamps. The $\mathrm{BJD_{UTC}}$ system accounts for light travel time based on the position of the target and the observer with respect to the Solar System barycenter at the time of observation. As the position of HST is constantly changing we set the position of the observer to be the center of the Earth at the time of observation, for which a small discrepancy of ± 23 milliseconds is introduced. This discrepancy can be safely ignored for our purposes.

While the telescope performed nominally throughout the observation, three well-documented sources of systematic error are present in our data that require removal. First, thermal fluctuations due to the spacecraft's orbit lead to clear brightness changes across the entire CCD (sometimes referred to as "breathing"), which are corrected for by subtracting image-median

fluxes (see the Supplementary Materials for details). After computing an optimal aperture for the target, we observe a strong intra-orbit ramping effect (also known as the "hook") in the white light curve (see Figure 2), which has been previously attributed to charge trapping in the CCD (*22, 23*). We initially tried a standard parametric approach for correcting these ramps using an exponential function, but found the result to be sub-optimal. Instead, we devised a new non-parametric approach described in the Supplementary Materials which substantially out-performs the previous approach.

We achieve a final mean intra-orbit precision of 375.5 ppm (versus 440.1 ppm using exponential functions), which is approximately 3.8 times more precise than *Kepler* when correcting for exposure time. The transit of Kepler-1625b is clearly observed even before the hook correction. After removal of the hooks, an apparent second decrease in brightness appears towards the end of the observations, which is evident even in the noisier exponential ramp corrected data (see Figure 2). Repeating our analysis for the only other bright star fully on the CCD, KIC4760469, reveals no peculiar behavior at this time indicating that the dip is not due to an instrumental common mode. Similarly, the centroids of both the target and the comparison star show no anomalous change around this time (see figure in the Supplementary Materials). (

By correlating the observed centroid variations with flux for both the target and the comparison star, we estimate that the small centroid changes in the second visit should induce (via residual pixel sensitivity variations) a flux change of $\sim$20 ppm, and certainly < 100 ppm (see figure in the Supplementary Materials). Since the moon-like dip is $\sim$500 ppm, it appears highly improbable that this could explain the apparent dip. In conclusion, although we cannot absolutely claim the moon-like dip is not due to an instrumental effect, we have shown that neither an instrumental common mode nor a residual pixel sensitivity effect can explain the dip and thus we proceed under the assumption it is astrophysical in what follows (see the Supplementary Materials for more details on these tests).

Upon inspection of the HST images we identified a previously uncatalogued point source within 2 arcseconds of our target. The star resides at position angle 8.5 degrees East of North, with a derived *Kepler* magnitude of 22.65. Its faintness means that it produces negligible contamination to our target spectrum. We attribute its new identification to the fact that it is both exceptionally faint and so close to the target that it was always lost in the glare in other images. Utilizing a *Gaia*-derived distance to the target we find that, were this point source to be at the same distance, it would be within 4500 AU of Kepler-1625. It is not known if the two sources are physically associated, however. We estimate that the source contributes less than 1 part in 3000 to our final WFC3 white light curve and thus can be safely ignored.

In addition to the breathing and the hooks, a third well-known source of WFC3 systematic error we see is a visit-long trend (apparent in Figure 2). These trends have not yet been correlated to any physical parameter related to the WFC3 observations (*24*), and thus the conventional approach is a linear slope (e.g. (*25–27*)) although a quadratic model has been used in some instances (e.g. (*28, 29*)). The timescale of the variations are comparable to the transit itself and thus cannot be removed in isolation, rather any detrending model is expected to be covariant with the transit model. For this reason, it was necessary to perform the detrending regression simultaneous to the actual transits fits. We considered three possible trend models; linear, quadratic and exponential. All models include an extra parameter describing a flux offset between the 14^{th} and 15^{th} orbits. This is motivated by the fact that the spacecraft performed a full guide star acquisition at the beginning of the 15^{th} orbit (a new "visit"), and ends up placing the spectrum $\sim$0.1 pixels away from where it appeared during the first 14 orbits. Although the white light curve shows no obvious flux change at this time, the reddest channels display substantial shifts motivating this offset term.

Finally, we extract light curves in nine wavelength bins across the spectrum in an attempt to perform transmission spectroscopy. As a planet transits its host star, the atmosphere may absorb

different amounts of light depending on the constituent molecules and their abundances (*30*). This makes the planet's transit depth wavelength-dependent. An accurate measurement of these transit depths not only provides the potential to characterize the atmosphere's composition; it is also potentially useful in providing an independent measurement of the planet's mass (*31*). While a low surface gravity planet will show very pronounced molecular features and a steep slope at short wavelengths due to Rayleigh scattering, a high surface gravity world will yield a substantially flatter transmission spectrum.

With the HST WFC3 data prepared, we are ready to combine it with the revised *Kepler* data in order to regress candidate models and compare between them. We considered four different transit models, which when combined with three different visit-long trend models, leads to a total of 12 models to evaluate. The four transit models here were designated as P, for the planet-only model; T, for a model that fits the observed transit timing variations (TTVs) in the system agnostically; Z, for a zero-radius moon model, which may produce all the gravitational effects of an exomoon without the flux reductions of a moon transit; and M, which is the full planet plus moon model. Models are generated using the `LUNA` photodynamical software package (*21*) and regression is performed via the multimodal nested sampling algorithm MULTINEST (*32, 33*). For each model, we not only derive the joint *a posteriori* parameter samples, but also a Bayesian evidence (also known as the marginal likelihood) enabling direct calculation of the Bayes factor between models.

One clear result from our analysis is that the HST transit of Kepler-1625b occurred $\simeq$72 minutes earlier than expected, indicating transit timing variations in the system. Bayes factors between models P and T support this for any choice of detrending model (see Table 1), with the T fits returning a χ^2 decreased by 17 to 19 (for 1048 data points). Further, if we fit the *Kepler* data in isolation and make predictions for the HST transit time, the observed time is $> 3\,\sigma$ discrepant (see figure in the Supplementary Materials). Identifying TTVs was among the first

methods proposed to discover exomoons (*8*), but certainly perturbations from an unseen planet could also be responsible. We find that the $\simeq$25 minute amplitude TTV can be explained by an external perturbing planet (see the Supplementary Materials), though with only four transits on hand it is not possible to constrain the mass or location of such a planet, and no other planet has been observed so far in the system.

We also found that model Z consistently out-performs model T, though the improvement to the fits is smaller at $\Delta\chi^2 \simeq$ 2-5 (see Table 1). This suggests that the evidence for the moon based on timing effects alone goes beyond the TTVs, providing modest evidence in favor of additional dynamical effects such as duration changes (*9*) and/or impact parameter variation (*10*), both expected consequences of a moon present in the system. This by itself would not constitute a strong enough case for a moon detection claim, but we consider it to be an important additional check that a real exomoon would be expected to pass.

The most compelling piece of evidence for an exomoon would be an exomoon transit, in addition to the observed TTV. If Kepler-1625b's early transit were indeed due to an exomoon, then we should expect the moon to transit late on the opposite side of the barycenter. The previously mentioned existence of an apparent flux decrease towards the end of our observations is therefore where we would expect it to be under this hypothesis. Although we have established that this dip is most likely astrophysical, as yet we have not discussed its significance, nor its compatibility with a self-consistent moon model.

We find that our self-consistent planet+moon models (M) always out-perform all other transit models in terms of maximum likelihood and Bayesian evidences (see Table 1). The presence of a TTV and an apparent decrease in flux at the correct phase position together make for a compelling case for an exomoon at this point. However, as is apparent from Figure 3, the amplitude and shape of the putative exomoon transit varies somewhat between the trend models, leading to both distinct model evidences and associated system parameters.

Although the overall preference of the moon model is arguably best framed by comparison to model P, the significance of the moon-like transit alone is best framed by comparing M and Z alone. Such a comparison reveals a strong dependency on the implied significance to the trend model used. In the worst case, we have the quadratic model with $2 \log K \simeq 4$, corresponding to "positive evidence" (*34*) - although we note the absolute evidence $\mathcal{Z}_M$ is the worst amongst the three. The linear model is far more optimistic yielding $2 \log K \simeq 18$, corresponding to "very strong evidence" (*34*), whereas the exponential sits between these extremes. The question then arises, which of our trend models is the correct one?

Because the linear model is a nested version of the quadratic model, and both models are linear with respect to time, it is more straight-forward to compare these two. The quadratic model essentially recovers the linear model, apparent from Figure 3, with a curvature within $1.5\,\sigma$ of zero, and yields almost the same best χ^2 score to within 1.2. This lack of meaningful improvement causes the log evidence to drop by 2.8, since evidences penalize wasted prior volume. The exponential model appears more competitive with a log evidence 1.72 lower, but a direct comparison of two different classes of models, such as these, is muddied by the fact that such analyses are sensitive to the choice of priors. The most useful comparison here is simply to state that the maximum likelihoods are within $\Delta\chi^2 = 0.68$ of one another and thus are likely equally justified from data-driven perspective.

Another approach we considered is to weigh the trend models uses the posterior samples. Given a planet or moon's mass, there is probabilistic range of expected radii based on empirical mass-radius relations (*35*). Although we exclude extreme densities in our fits, parameters from model M can certainly lead to improbable solutions with regards to the photodynamically inferred (*36*) masses and radii.

To investigate this, we inferred the planetary mass using two methods for each model and evaluated their self-consistency. The first method combines the photodynamically-inferred

planet-to-star mass ratio (*36*) with a prediction for the mass based on the well-constrained radius using `forecaster`; an empirical probabilistic mass-radius relation (*35*). The second method approaches the problem from the other side, taking the moon's radius and predicting its mass with `forecaster` then calculating the planetary mass via the photodynamically-inferred moon-to-planet mass ratio. Our analysis (discussed in more detail in the Supplementary Materials) reveals that all three models have physically plausible solutions and generally converge at $\sim 10^3\, M_\oplus$ for the planetary mass, with the exception of the quadratic model had broader support extending down to Saturn-mass. We ultimately combined the two mass estimates to provide a final best-estimate for each model in Table 2.

As a consistency check, we used our derived transmission spectrum to constrain the allowed range of planetary masses for a cloudless atmosphere (*31*). Using an MCMC with `Exo-Transmit` (*38*), we find masses in the range of > 0.4 Jupiter masses (to 95% confidence) are consistent with the nearly flat spectrum observed, assuming a cloudless atmosphere (see the Supplementary Materials for details).

In conclusion, the linear and exponential models appear to be the most justified by the data and also lead to slightly improved physical self-consistency, although we certainly cannot exclude the quadratic model at this time. For this reason, we elected to present the associated system parameters resulting from all three models in Table 2. The maximum *a posteriori* solutions from each, using model M, are presented in Figure 4 for reference.

We briefly comment on some of the inferred physical parameters for this system. First, we have assumed a circular moon orbit throughout due to the likely rapid effects of tidal circularization. However, we did allow the moon to explore three-dimensional orbits and find some evidence for non-coplanarity. Our solution favors a moon orbit tilted by about 45 degrees to the planet's orbital plane, with both pro- and retrograde solutions being compatible. The only comparable known large moon with such an inclined orbit is Triton around Neptune, which is

generally thought to be a captured Kuiper Belt object (*39*). However, we caution that the constraints here are weak, reflected by the posterior's broad shape, and thus it would be unsurprising if the true answer is in fact coplanar.

One jarring aspect of the system is the sheer scale of it. The exomoon has a radius of $\simeq 4\,R_\oplus$, making it very similar to Neptune or Uranus in size. The measured mass, including the `forecaster` constraints, comes in at $\log(M_S/M_\oplus) = (1.2 \pm 0.3)\,M_\oplus$, which is again compatible with Neptune or Uranus (although note that this solution is in part informed by an empirical mass-radius relation). This Neptune-like moon orbits a planet with a size fully compatible with that of Jupiter at $(11.4 \pm 1.5)\,R_\oplus$, but most likely a few times more massive. Finally, although the moon's period is highly degenerate and multimodal, we find the semi-major axis is relatively wide at $\simeq$40 planetary radii. With a Hill radius of (200 ± 50) planetary radii, this is well within the Hill sphere and expected region of stability.

The blackbody equilibrium temperature of the planet and moon, assuming zero albedo, is $\sim$350 K. Adopting a more realistic albedo can drop this down to ~ 300 K. Of course, as a likely gaseous pair of objects there is not much prospect of habitability here, although it appears that the moon can indeed be in the temperature zone for optimistic definitions of the habitable zone.

What is particularly interesting about the star is that it appears to be a Solar mass star evolving off the main sequence. This inference is supported a recent analysis of the *Gaia* DR2 parallax by (*40*), as well as our own isochrone fits (see the Supplementary Materials). We find that the star is certainly older than than Sun, at $\simeq$10 Gyr in age, and that insolation at the location of the system was thus lower in the past. The luminosity was likely close to Solar for most of the star's life, making the equilibrium temperature drop down to $\sim$250 K for Jovian albedos for most of its existence. The old age of the system also implies plenty of time for tidal evolution, which could explain why we find the moon at a fairly wide orbital separation.

The origins of such a system can only be speculated upon at this time. A mass ratio of 1.5%

is certainly not unphysical from in-situ formation using gas-starved disk models, but it does represent the very upper end of what numerical simulations form (*37*). In such a scenario, a separate explanation for the tilt would be required. Impacts between gaseous planets leading to captured moons is not well-studied but could be worth further investigation. A binary exchange mechanism would be challenged by the requirement for a Neptune to be in an initial binary with comparably mass object, such as a Super-Earth (*39*). Formation of an initial binary planet, perhaps through tidal capture, seems improbable due to the tight orbits simulation work tends to produce from such events (*41*). If confirmed, Kepler-1625b-i will certainly provide an interesting puzzle for theorists to solve.

Taken together, a detailed investigation of a suite of models tested in this work suggest that the exomoon hypothesis is the best explanation to the presently available observations. The two main pieces of information driving this result are i) a strong case for TTVs, in particular a 72 minute early transit observed during our HST observations and ii) a moon-like transit signature apparent even in the pre-detrended data. We also note that we find a modestly improved evidence when including additional dynamical effects induced by moons aside from TTVs.

The exomoon hypothesis is further strengthened by our analysis which demonstrates that a) the moon-like transit is not due to an instrumental common mode nor residual pixel sensitivity variations; b) the moon-like transit occurs at the correct phase position to also explain the observed TTV; and c) simultaneous detrending and photodynamical modeling retrieves a solution which is not only favored by the data, but is also physically self-consistent.

Put together, these points make for a compelling case for an exomoon around Kepler-1625b. It also represents the simplest hypothesis to explain both the TTV and the post-transit flux decrease, since other solutions would require two separate and unconnected explanations for these two observations.

There remains some aspects of our present interpretation of the data that give us pause.

First, the moon's Neptunian size and inclined orbit are peculiar, though it is difficult to assess how likely this is *a priori* since no previously known exomoons exist. Second, the moon's transit occurs towards the end of the observations and more out-of-transit data could have more cleanly resolved this signal. Nevertheless, we highlight that no centroid shifts nor flux changes in our comparison star are found around this time, and thus the dip appears astrophysical in nature. Third, the moon's inferred properties are sensitive to the model used for correcting HST's visit-long trend and thus some uncertainty remains regarding the true system properties. However, the solution we deem most likely, a linear visit-long trend, also represents the most widely agreed upon solution for the visit-long trend in the literature.

Finally, it is somewhat ironic that the case for observing Kepler-1625b with HST was contingent on a previous data release of the *Kepler* photometry which indicated a moon (*12*), while the most recent data release only modestly favors that hypothesis when treated in isolation. Despite this, we would argue that planets like Kepler-1625b were always ideal targets for exomoon follow-up, being a Jupiter-sized planet on a wide, circular orbit around a Solar-mass star. There are certainly hints of the moon present even in the revised *Kepler* data, but it is the HST data - with a precision four times superior to *Kepler*- which is critical to the driving the moon as the favored model. These points suggest that it would be worthwhile to pursue similar *Kepler* planets for exomoons with HST or other facilities, even if the *Kepler* data alone do not show large moon-like signatures. Furthermore, our work demonstrates how impactful the changes to *Kepler* photometry were, at least in this case, as it suggests other results over the course of the *Kepler* mission may be similarly impacted, particularly for small signals.

All in all, it is difficult to assign a precise probability to the reality of Kepler-1625b-i. Formally, the preference for the moon model over the planet-only model is very high, with a Bayes factor exceeding 400,000. On the other hand, this is a complicated and involved analysis where a minor effect unaccounted for, or anomalous artefact, could potentially change our interpreta-

tion. In short, it is the unknown unknowns that we cannot quantify. These reservations exist because this would be a first of its kind detection - the first exomoon. Historically, the first exoplanet claims faced great skepticism because there was simply no precedence for them. If many more exomoons are detected in the coming years with similar properties to Kepler-1625b-i, it would hardly be a controversial claim to add one more. Ultimately, Kepler-1625b-i cannot be considered confirmed until it has survived the long scrutiny of many years, observations and community skepticism, as well as perhaps the detection of similar such objects. Despite this, it is an exciting reminder of how little we really know about distant planetary systems and the great spirit of discovery exoplanetary science embodies.

References and Notes

1. Han, C., Han, W. 2002. On the Feasibility of Detecting Satellites of Extrasolar Planets via Microlensing. The Astrophysical Journal 580, 490.

2. Han, C. 2008. Microlensing Detections of Moons of Exoplanets. The Astrophysical Journal 684, 684.

3. Liebig, C. 2010. Detectability of Extrasolar Moons as Gravitational Microlenses. Astronomy & Astrophysics 520, 68.

4. Cabrera, J., Schneider, J. 2007. Detecting companions to extrasolar planets using mutual events. Astronomy and Astrophysics 464, 1133.

5. Agol, E., Jansen, T., Lacy, B., Robinson, T. D., Meadows, V. 2015. The Center of Light: Spectroastrometric Detection of Exomoons. The Astrophysical Journal 812, 5.

6. Noyola, J. P., Satyal, S., Musielak, Z. E. 2014. Detection of Exomoons through Observation of Radio Emissions. The Astrophysical Journal 791, 25.

7. Lewis, K. M., Sackett, P. D., Mardling, R. A. 2008. Possibility of Detecting Moons of Pulsar Planets through Time-of-Arrival Analysis. The Astrophysical Journal 685, L153.

8. Sartoretti, P., Schneider, J. 1999. On the detection of satellites of extrasolar planets with the method of transits. Astronomy and Astrophysics Supplement Series 134, 553.

9. Kipping, D. M. 2009. Transit timing effects due to an exomoon. Monthly Notices of the Royal Astronomical Society 392, 181.

10. Kipping, D. M. 2009. Transit timing effects due to an exomoon - II. Monthly Notices of the Royal Astronomical Society 396, 1797.

11. Barclay, T., and 57 colleagues 2013. A sub-Mercury-sized exoplanet. Nature 494, 452.

12. Teachey, A., Kipping, D. M., Schmitt, A. R. 2018. HEK. VI. On the Dearth of Galilean Analogs in Kepler, and the Exomoon Candidate Kepler-1625b I. The Astronomical Journal 155, 36.

13. Namouni, F. 2010. The Fate of Moons of Close-in Giant Exoplanets. The Astrophysical Journal 719, L145.

14. Spalding, C., Batygin, K., Adams, F. C. 2016. Resonant Removal of Exomoons during Planetary Migration. The Astrophysical Journal 817, 18.

15. Morton, T. D., and 7 colleagues 2016. False Positive Probabilities for all Kepler Objects of Interest: 1284 Newly Validated Planets and 428 Likely False Positives. The Astrophysical Journal 822, 86.

16. Mathur, S., and 16 colleagues 2017. Revised Stellar Properties of Kepler Targets for the Q1-17 (DR25) Transit Detection Run. The Astrophysical Journal Supplement Series 229, 30.

17. Jenkins, J. M., and 29 colleagues 2010. Overview of the Kepler Science Processing Pipeline. The Astrophysical Journal 713, L87.

18. Kipping, D. M., Hartman, J., Buchhave, L. A., Schmitt, A. R., Bakos, G. Á., Nesvorný, D. 2013. The Hunt for Exomoons with Kepler (HEK). II. Analysis of Seven Viable Satellite-hosting Planet Candidates. The Astrophysical Journal 770, 101.

19. Stumpe, M. C., and 10 colleagues 2012. Kepler Presearch Data Conditioning I—Architecture and Algorithms for Error Correction in Kepler Light Curves. Publications of the Astronomical Society of the Pacific 124, 985.

20. Smith, J. C., and 10 colleagues 2012. Kepler Presearch Data Conditioning II - A Bayesian Approach to Systematic Error Correction. Publications of the Astronomical Society of the Pacific 124, 1000.

21. Kipping, D. M. 2011. LUNA: an algorithm for generating dynamic planet-moon transits. Monthly Notices of the Royal Astronomical Society 416, 689.

22. Agol, E., and 6 colleagues 2010. The Climate of HD 189733b from Fourteen Transits and Eclipses Measured by Spitzer. The Astrophysical Journal 721, 1861.

23. Berta, Z. K., and 9 colleagues 2012. The Flat Transmission Spectrum of the Super-Earth GJ1214b from Wide Field Camera 3 on the Hubble Space Telescope. The Astrophysical Journal 747, 35.

24. Wakeford, H. R., Sing, D. K., Evans, T., Deming, D., Mandell, A. 2016. Marginalizing Instrument Systematics in HST WFC3 Transit Light Curves. The Astrophysical Journal 819, 10.

25. Huitson, C. M., and 16 colleagues 2013. An HST optical-to-near-IR transmission spectrum of the hot Jupiter WASP-19b: detection of atmospheric water and likely absence of TiO. Monthly Notices of the Royal Astronomical Society 434, 3252.

26. Ranjan, S., and 6 colleagues 2014. Atmospheric Characterization of Five Hot Jupiters with the Wide Field Camera 3 on the Hubble Space Telescope. The Astrophysical Journal 785, 148.

27. Knutson, H. A., and 9 colleagues 2014. Hubble Space Telescope Near-IR Transmission Spectroscopy of the Super-Earth HD 97658b. The Astrophysical Journal 794, 155.

28. Stevenson, K. B., and 7 colleagues 2014. Transmission Spectroscopy of the Hot Jupiter WASP-12b from 0.7 to 5 μm. The Astronomical Journal 147, 161.

29. Stevenson, K. B., Bean, J. L., Fabrycky, D., Kreidberg, L. 2014. A Hubble Space Telescope Search for a Sub-Earth-sized Exoplanet in the GJ 436 System. The Astrophysical Journal 796, 32.

30. Seager, S., Sasselov, D. D. 2000. Theoretical Transmission Spectra during Extrasolar Giant Planet Transits. The Astrophysical Journal 537, 916.

31. de Wit, J., Seager, S. 2013. Constraining Exoplanet Mass from Transmission Spectroscopy. Science 342, 1473.

32. Feroz, F., Hobson, M. P. 2008. Multimodal nested sampling: an efficient and robust alternative to Markov Chain Monte Carlo methods for astronomical data analyses. Monthly Notices of the Royal Astronomical Society 384, 449.

33. Feroz, F., Hobson, M. P., Bridges, M. 2009. MULTINEST: an efficient and robust Bayesian inference tool for cosmology and particle physics. Monthly Notices of the Royal Astronomical Society 398, 1601.

34. Kass, R. E. & Raftery, A. E. 1995. Bayes Factors. *Journal of the American Statistical Association*, 90, 773.

35. Chen, J., Kipping, D. 2017. Probabilistic Forecasting of the Masses and Radii of Other Worlds. The Astrophysical Journal 834, 17.

36. Kipping, D. M. 2010. How to weigh a star using a moon. Monthly Notices of the Royal Astronomical Society 409, L119.

37. Cilibrasi, M., Szulágyi, J., Mayer, L., Drażkowska, J., Miguel, Y., Inderbitzi, P. 2018. Satellites Form Fast & Late: a Population Synthesis for the Galilean Moons. ArXiv e-prints arXiv:1801.06094.

38. Kempton, E. M.-R., Lupu, R., Owusu-Asare, A., Slough, P., Cale, B. 2017. Exo-Transmit: An Open-Source Code for Calculating Transmission Spectra for Exoplanet Atmospheres of Varied Composition. Publications of the Astronomical Society of the Pacific 129, 44402.

39. Agnor, C. B., Hamilton, D. P. 2006. Neptune's capture of its moon Triton in a binary-planet gravitational encounter. Nature 441, 192.

40. Berger, T. A., Huber, D., Gaidos, E., van Saders, J. L. 2018. Revised Radii of Kepler Stars and Planets using Gaia Data Release 2. ArXiv e-prints arXiv:1805.00231.

41. Ochiai, H., Nagasawa, M., Ida, S. 2014. Extrasolar Binary Planets. I. Formation by Tidal Capture during Planet-Planet Scattering. The Astrophysical Journal 790, 92.

42. Dalba, P. A., Muirhead, P. S., Croll, B., Kempton, E. M.-R. 2017. Kepler Transit Depths Contaminated By a Phantom Star. The Astronomical Journal 153, 59.

43. Bryson, S. T., and 10 colleagues 2010. The Kepler Pixel Response Function. The Astrophysical Journal 713, L97.

44. Schlafly, E. F., Finkbeiner, D. P. 2011. Measuring Reddening with Sloan Digital Sky Survey Stellar Spectra and Recalibrating SFD. The Astrophysical Journal 737, 103.

45. Kümmel, M., Walsh, J. R., Pirzkal, N., Kuntschner, H., Pasquali, A. 2009. The Slitless Spectroscopy Data Extraction Software aXe. Publications of the Astronomical Society of the Pacific 121, 59.

46. Bertin, E., Arnouts, S. 2010. SExtractor: Source Extractor. Astrophysics Source Code Library ascl:1010.064.

47. Kümmel, M., Kuntschner, H., Walsh, J. R., Bushouse, H. 2011. Master sky images for the WFC3 G102 and G141 grisms.Space Telescope WFC Instrument Science Report.

48. Jones, E., Oliphant, T., Peterson, P., et al. 2001, http://www.scipy.org

49. Deming, D., and 20 colleagues 2013. Infrared Transmission Spectroscopy of the Exoplanets HD 209458b and XO-1b Using the Wide Field Camera-3 on the Hubble Space Telescope. The Astrophysical Journal 774, 95.

50. Deming, D., Harrington, J., Seager, S., Richardson, L. J. 2006. Strong Infrared Emission from the Extrasolar Planet HD 189733b. The Astrophysical Journal 644, 560.

51. Knutson, H. A., and 8 colleagues 2007. A map of the day-night contrast of the extrasolar planet HD 189733b. Nature 447, 183.

52. Charbonneau, D., and 7 colleagues 2008. The Broadband Infrared Emission Spectrum of the Exoplanet HD 189733b. The Astrophysical Journal 686, 1341.

53. Freedman, R. S., Marley, M. S., Lodders, K. 2008. Line and Mean Opacities for Ultracool Dwarfs and Extrasolar Planets. The Astrophysical Journal Supplement Series 174, 504.

54. Freedman, R. S., Lustig-Yaeger, J., Fortney, J. J., Lupu, R. E., Marley, M. S., Lodders, K. 2014. Gaseous Mean Opacities for Giant Planet and Ultracool Dwarf Atmospheres over a Range of Metallicities and Temperatures. The Astrophysical Journal Supplement Series 214, 25.

55. Lupu, R. E., and 8 colleagues 2014. The Atmospheres of Earthlike Planets after Giant Impact Events. The Astrophysical Journal 784, 27.

56. Luri, X., Brown, A. G. A., Sarro, L. M., et al. 2018, "Gaia Data Release 2: using Gaia parallaxes", arXiv e-print:1804.09376

57. Morton, T. 2015, isochrones: Stellar model grid package, Astrophysics Source Code Library.

58. Foreman-Mackey, D., Hogg, D. W., Lang, D., Goodman, J. 2013, "emcee: The MCMC Hammer", PASP, 125, 306.

59. Huber, D., Bryson, S. T., Haas, M. R., et al. 2016, "The K2 Ecliptic Plane Input Catalog (EPIC) and Stellar Classifications of 138,600 Targets in Campaigns 1-8", ApJS, 224, 2.

60. Kipping, D. M., Bakos, G. Á., Buchhave, L., Nesvorný, D., Schmitt, A. 2012. The Hunt for Exomoons with Kepler (HEK). I. Description of a New Observational project. The Astrophysical Journal 750, 115.

61). Skilling, J. 2004. Nested Sampling. American Institute of Physics Conference Series 395.

62. Kipping, D. M. 2013. Efficient, uninformative sampling of limb darkening coefficients for two-parameter laws. Monthly Notices of the Royal Astronomical Society 435, 2152.

63. Kipping, D. M., and 7 colleagues 2015. The Hunt for Exomoons with Kepler (HEK): V. A Survey of 41 Planetary Candidates for Exomoons. The Astrophysical Journal 813, 14.

64. Agol, E., Deck, K. 2016. TTVFaster: First order eccentricity transit timing variations (TTVs). Astrophysics Source Code Library ascl:1604.012.

65. Carter, J. A., Yee, J. C., Eastman, J., Gaudi, B. S., Winn, J. N. 2008. Analytic Approximations for Transit Light-Curve Observables, Uncertainties, and Covariances. The Astrophysical Journal 689, 499.

66. Nesvorný, D., Kipping, D., Terrell, D., Hartman, J., Bakos, G. Á., Buchhave, L. A. 2013. KOI-142, The King of Transit Variations, is a Pair of Planets near the 2:1 Resonance. The Astrophysical Journal 777, 3.

67. Szabó, G. M., Pál, A., Derekas, A., Simon, A. E., Szalai, T., Kiss, L. L. 2012. Spin-orbit resonance, transit duration variation and possible secular perturbations in KOI-13. Monthly Notices of the Royal Astronomical Society 421, L122.

68. Kipping, D. M. 2014. Characterizing distant worlds with asterodensity profiling. Monthly Notices of the Royal Astronomical Society 440, 2164.

69. Agnor, C. B., Hamilton, D. P. 2006. Neptune's capture of its moon Triton in a binary-planet gravitational encounter. Nature 441, 192.

Acknowledgements

1. The authors wish to thank STScI staff scientists Bill Januszewski and Kevin Stevenson for their critical contributions during the planning and execution of the HST observation. We also thank Jon Jenkins at NASA and Paul Dalba at Boston University for useful discussions regarding source contamination in the *Kepler* data. Members of the Cool Worlds Lab at Columbia University (Ruth Angus, Jingjing Chen, Jorge Cortes, Tiffany Jansen, Moiya McTier, Emily Sandford, and Adam Wheeler) provided valuable feedback at every stage of this analysis. We are also grateful to members of the HEK project for their continued support throughout the early years of our program. Finally, we thank Travis Berger and collaborators for sharing their *Gaia*-derived posteriors for the target's radius.

1. **Funding and Support:** Analysis was carried out in part on the NASA Supercomputer PLEIADES (Grant #HEC-SMD-17-1386). AT is supported through the NSF Graduate Research Fellowship (DGE 16-44869). DK is supported by the Alfed P. Sloan Foundation Fellowship. This work is based in part on observations made with the NASA/ESA Hubble Space Telescope, obtained at the Space Telescope Science Institute, which is operated by the Association of Universities for Research in Astronomy, Inc., under NASA contract NAS 5-26555. These observations are associated with program #GO-15149. Support for program #GO-15149 was provided by NASA through a grant from the Space Telescope Science Institute, which is operated by the Association of Universities for Research in Astronomy, Inc., under NASA contract NAS 5-26555. This paper includes data collected by the *Kepler* Mission. Funding for the *Kepler* Mission is provided by the NASA Science Mission directorate. This research has made use of the Exoplanet Follow-up Observation Program website, which is operated by the California Institute of Technology, under contract with the National Aeronautics and Space Administration under the Exoplanet Exploration Program.

1. **Software** This work made use of Numpy, Scipy, Pandas, Matplotlib, Astropy, `TTVfaster`, `Exo-Transmit`, `forecaster`, `LUNA` and MULTINEST.

List of Supplementary Materials

1. Materials and Methods
2. Tables S1-S4
3. Figures S1-S12
4. References (42-69)

Table 1: Bayesian evidences ($\mathcal{Z}$) and maximum likelihoods ($\hat{\mathcal{L}}$) from our combined fits using *Kepler* and new HST data. Kepler+HST fits. The subscripts are P for planet model, T for planetary TTV model, Z for a zero-radius moon model and M for moon model. The three columns are for each trend model attempted.

	linear	quadratic	exponential
$\log \mathcal{Z}_{\rm P}$	6302.79 ± 0.11	6306.68 ± 0.11	6308.41 ± 0.11
$\log \mathcal{Z}_{\rm T}$	6304.86 ± 0.11	6308.81 ± 0.12	6305.11 ± 0.11
$\log \mathcal{Z}_{\rm Z}$	6306.84 ± 0.11	6311.12 ± 0.12	6310.82 ± 0.12
$\log \mathcal{Z}_{\rm M}$	6315.73 ± 0.12	6312.92 ± 0.12	6314.01 ± 0.12
$2\log K(\mathcal{Z}'_{\rm M}/\mathcal{Z}'_{\rm P})$	1.00 ± 0.22		
$2\log(\mathcal{Z}_{\rm M}/\mathcal{Z}_{\rm P})$	25.88 ± 0.32	12.47 ± 0.33	11.19 ± 0.32
$2\log(\mathcal{Z}_{\rm M}/\mathcal{Z}_{\rm T})$	21.72 ± 0.33	8.21 ± 0.34	17.81 ± 0.33
$2\log(\mathcal{Z}_{\rm M}/\mathcal{Z}_{\rm Z})$	17.77 ± 0.33	3.61 ± 0.33	6.38 ± 0.34
$\Delta\chi'^2_{\rm PM} = 2\log(\hat{\mathcal{L}}'_{\rm M}/\hat{\mathcal{L}}'_{\rm P})$	18.66		
$\Delta\chi^2_{\rm PM} = 2\log(\hat{\mathcal{L}}_{\rm M}/\hat{\mathcal{L}}_{\rm P})$	54.93	41.04	41.57
$\Delta\chi^2_{\rm TM} = 2\log(\hat{\mathcal{L}}_{\rm M}/\hat{\mathcal{L}}_{\rm T})$	35.69	23.97	38.71
$\Delta\chi^2_{\rm ZM} = 2\log(\hat{\mathcal{L}}_{\rm M}/\hat{\mathcal{L}}_{\rm Z})$	33.68	19.59	19.22

Table 2: Median and $\pm 34.1\%$ quantile range of the *a posteriori* model parameters from model M, where each column defined a different visit-long trend model. Top panel gives the credible intervals for the actual parameters used in the fit, and the lower panel gives a selection of relevant derived parameters conditioned upon our revised stellar parameters. The quoted inclination of the satellite is the inclination modulo 90 degrees.

parameter	linear	quadratic	exponential
photodynamics only			
$R_{P,\mathrm{Kep}}/R_\star$	$0.06075^{+0.00062}_{-0.00065}$	$0.06061^{+0.00068}_{-0.00073}$	$0.06072^{+0.0062}_{-0.00063}$
$R_{P,\mathrm{HST}}/R_{P,\mathrm{Kep}}$	$0.998^{+0.013}_{-0.013}$	$1.009^{+0.019}_{-0.017}$	$1.006^{+0.014}_{-0.014}$
$\rho_{\star,\mathrm{LC}}$ [g cm^{-3}]	424^{+9}_{-16}	424^{+9}_{-15}	425^{+9}_{-14}
b	$0.104^{+0.084}_{-0.066}$	$0.099^{+0.088}_{-0.063}$	$0.096^{+0.078}_{-0.058}$
P_P [days]	$287.37278^{+0.00075}_{-0.00065}$	$287.3727^{+0.0022}_{-0.0015}$	$287.37269^{+0.00074}_{-0.00076}$
τ_0 [BJD$_{\mathrm{UTC}}$]	$2456043.9587^{+0.0027}_{-0.0027}$	$2456043.9572^{+0.0033}_{-0.0093}$	$56043.9585^{+0.0025}_{-0.0029}$
$q_{1,\mathrm{Kep}}$	$0.45^{+0.19}_{-0.14}$	$0.44^{+0.19}_{-0.15}$	$0.45^{+0.18}_{-0.14}$
$q_{2,\mathrm{Kep}}$	$0.31^{+0.19}_{-0.15}$	$0.32^{+0.20}_{-0.16}$	$0.31^{+0.19}_{-0.15}$
$q_{1,\mathrm{HST}}$	$0.087^{+0.057}_{-0.041}$	$0.096^{+0.064}_{-0.045}$	$0.087^{+0.056}_{-0.040}$
$q_{2,\mathrm{HST}}$	$0.25^{+0.25}_{-0.15}$	$0.21^{+0.23}_{-0.14}$	$0.22^{+0.22}_{-0.14}$
P_S [days]	22^{+17}_{-9}	24^{+18}_{-11}	22^{+15}_{-9}
a_{SP}/R_P	45^{+10}_{-5}	36^{+10}_{-13}	42^{+7}_{-4}
ϕ_S [°]	179^{+136}_{-70}	141^{+161}_{-65}	160^{+150}_{-60}
i_S [°]	42^{+15}_{-18}	49^{+21}_{-22}	43^{+15}_{-19}
Ω_S [°]	0^{+142}_{-83}	12^{+132}_{-113}	8^{+136}_{-81}
(M_S/M_P)	$0.0141^{+0.0048}_{-0.0039}$	$0.0196^{+0.0294}_{-0.0071}$	$0.0149^{+0.0052}_{-0.0038}$
$(R_S/R_P)^*$	$0.431^{+0.033}_{-0.036}$	$0.271^{+0.150}_{-0.099}$	$0.363^{+0.048}_{-0.079}$
Δa_0 [ppm]	330^{+120}_{-120}	180^{+170}_{-210}	220^{+130}_{-140}
+ stellar properties			
$R_\star$ [$R_\odot$]	$1.73^{+0.24}_{-0.22}$	$1.73^{+0.24}_{-0.22}$	$1.73^{+0.24}_{-0.22}$
$M_\star$ [$M_\odot$]	$1.04^{+0.08}_{-0.06}$	$1.04^{+0.08}_{-0.06}$	$1.04^{+0.08}_{-0.06}$
$\rho_{\star,\mathrm{iso}}$ [kg m^{-3}]	$0.29^{+0.13}_{-0.09}$	$0.29^{+0.13}_{-0.09}$	$0.29^{+0.13}_{-0.09}$
$e^\dagger_{\mathrm{min}}$	$0.13^{+0.11}_{-0.09}$	$0.13^{+0.11}_{-0.09}$	$0.13^{+0.11}_{-0.09}$
R_P [$R_\oplus$]	$11.4^{+1.6}_{-1.5}$	$11.4^{+1.6}_{-1.4}$	$11.4^{+1.6}_{-1.4}$
$\log_{10}(M_P/M_\odot)$	$2.86^{+0.48}_{-0.50}$	$2.40^{+0.70}_{-0.72}$	$2.75^{+0.53}_{-0.54}$
a_P [AU]	$0.98^{+0.14}_{-0.13}$	$0.98^{+0.14}_{-0.12}$	$0.98^{+0.14}_{-0.12}$
R_S [$R_\oplus$]	$4.90^{+0.79}_{-0.72}$	$3.09^{+1.71}_{-1.19}$	$4.05^{+0.86}_{-1.01}$
$\log_{10}(M_S/M_\odot)$	$1.00^{+0.46}_{-0.48}$	$0.74^{+0.56}_{-0.52}$	$0.93^{+0.49}_{-0.50}$
S_{eff} [$S_\oplus$]	$2.65^{+0.19}_{-0.16}$	$2.64^{+0.18}_{-0.16}$	$2.64^{+0.18}_{-0.16}$
+ forecaster			
$\log_{10}(M_P/M_\odot)$	$3.12^{+0.26}_{-0.27}$	$2.65^{+0.50}_{-0.52}$	$3.01^{+0.26}_{-0.30}$
$\log_{10}(M_S/M_\odot)$	$1.27^{+0.29}_{-0.30}$	$1.11^{+0.55}_{-0.58}$	$1.20^{+0.32}_{-0.34}$
M_P [M_J]	$[1.2, 12.5]$	$[0.2, 9.0]$	$[0.6, 10.5]$
M_S [$M_\odot$]	$[4.4, 68]$	$[1.0, 140]$	$[2.6, 76]$
K [m/s]	$[35, 380]$	$[6, 280]$	$[18, 320]$

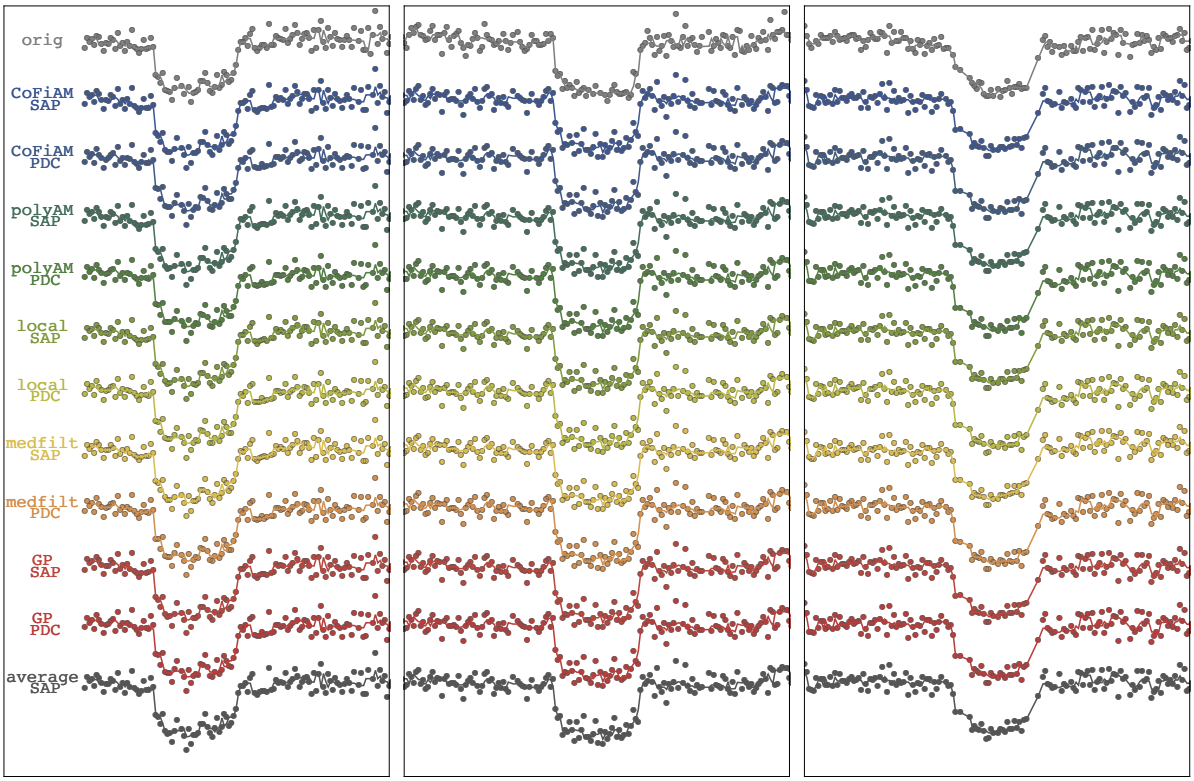

Figure 1: Comparison of five different methods used for detrending the `SAP` *Kepler* data. Baselines shown represent the full training set used, except for the `local` method which is trained on only data immediately surrounding the transits of interest.

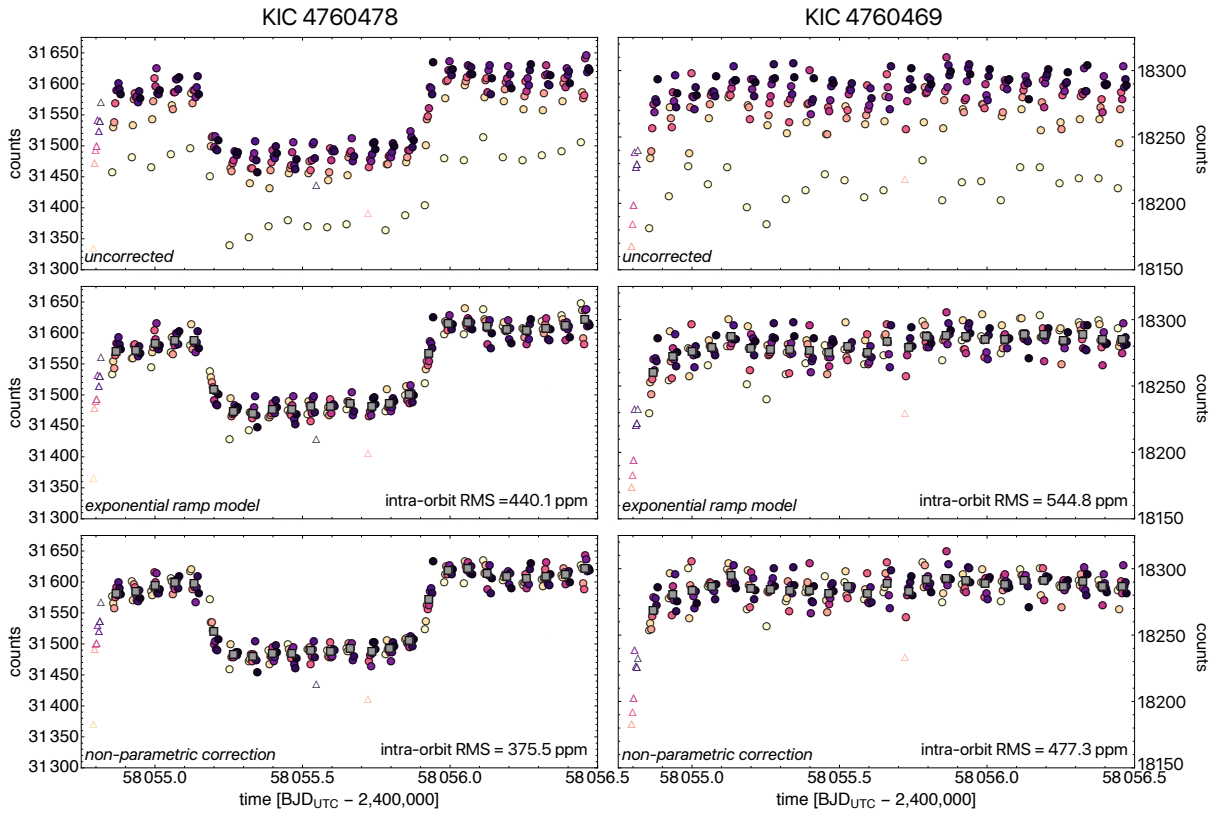

Figure 2: Top row shows the optimal aperture photometry of our target (left) and the best comparison star (right), where the hooks and visit-long trends are clearly present. Points are colored by their exposure number within each HST orbit (triangles represent outliers). Middle row shows a hook-correction using the common exponential ramp model on both stars. Bottom row shows the result from an alternative and novel hook-correction approach introduced in this work.

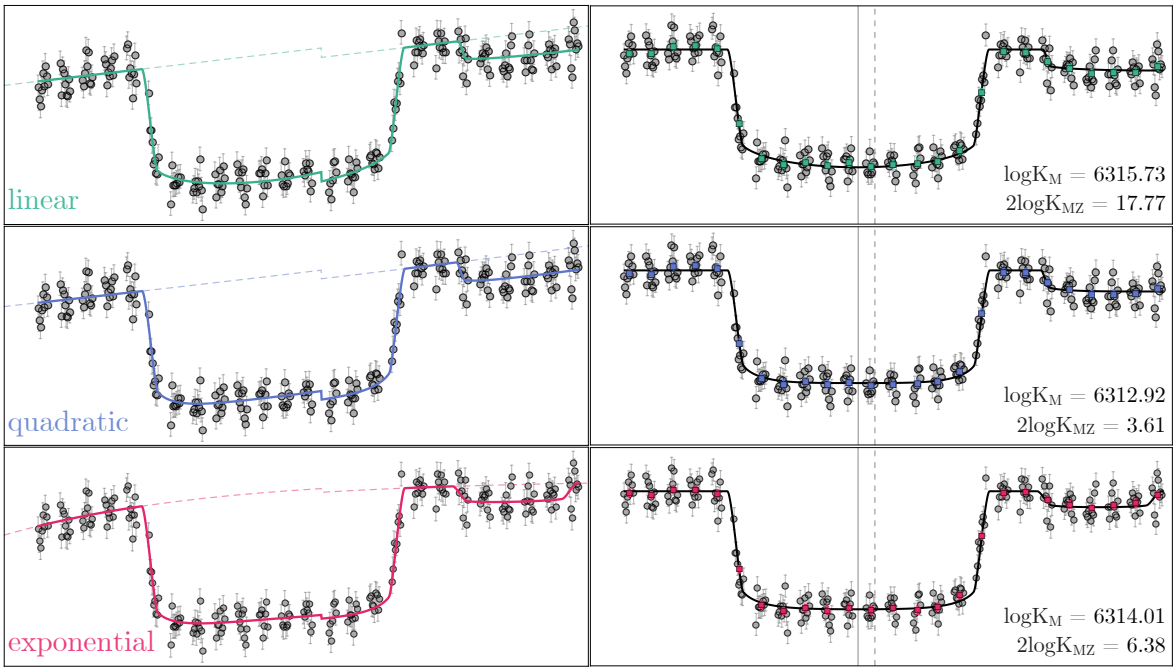

Figure 3: The HST observations with three proposed trends fit to the data (left) and with the trends removed (right). Bottom-right numbers in each row give the Bayes factor between a planet+moon model (model M) and a planet+moon model where the moon radius equals zero (model Z), which tracks the significance of the moon-like dip in isolation.

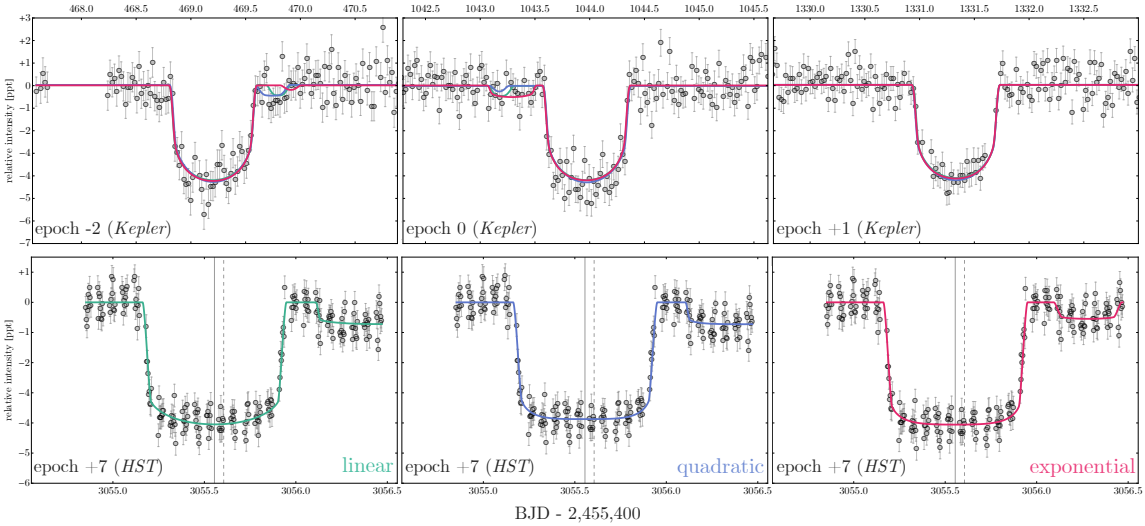

Figure 4: The three transits in *Kepler* (top) and the October 2017 transit observed with HST (bottom) for three three trend model solutions. The three colored lines show the three corresponding trend model solutions for model M, our favored transit model. The shape of the HST transit differs from the *Kepler* transits due to limb darkening differences between the bandpasses.